Design and Installation of a Hybrid-Spar Floating Wind Turbine Platform

Utsunomiya, Tomoaki
Department of Ocean Energy Resources, Faculty of Engineering, Kyushu University : Professor

Sato, Iku
Toda Corporation

Kobayashi, Osamu
Toda Corporation

Shiraishi, Takashi
Hitachi, Ltd.

他

出版情報：Proceedings of the ASME 2015 34th International Conference on Ocean, Offshore and Arctic Engineering, 2015-05-31
バージョン：
権利関係：

Proceedings of the ASME 2015 34th International Conference on Ocean, Offshore and Arctic Engineering
OMAE2015
May 31-June 5, 2015, St. John's, Newfoundland, Canada

OMAE2015-41544

DESIGN AND INSTALLATION OF A HYBRID-SPAR FLOATING WIND TURBINE PLATFORM

Tomoaki Utsunomiya
Kyushu University
Dept. of Ocean Energy Res.
Fukuoka 819-0395, Japan

Iku Sato
Toda Corporation
Kyobashi 1-7-1, Chuo-ku
Tokyo 104-8388, Japan

Osamu Kobayashi
Toda Corporation
Kyobashi 1-7-1, Chuo-ku
Tokyo 104-8388, Japan

Takashi Shiraishi
Hitachi, Ltd., Power Systems Company
Shirogane-cho 1-1-1, Hitachi
Ibaraki 317-0056, Japan

Takashi Harada
Hitachi, Ltd., Power Systems Company
Sotokanda 1-18-13, Chiyoda-ku
Tokyo 101-8608, Japan

ABSTRACT

A floating offshore wind turbine platform supporting a 2MW downwind-type turbine was successfully installed offshore of Kabashima Island, Goto city, Nagasaki prefecture, Japan on October 18, 2013. It has been operating since October 28, 2013 as the first grid-connected multi-megawatt floating wind turbine in Japan. The spar platform has a unique feature, that is, the upper part of the spar is made of steel (as usual) but the lower part is made of precast prestressed concrete (PC). Such a configuration is referred to as hybrid-spar. In this paper, the design methodology of the hybrid spar is presented - including environmental design conditions, DLCs (Design Load Cases), dynamic analysis, fatigue analysis, etc. Also, the installation procedure is presented briefly.

INTRODUCTION

Wind energy resources in Japan are now considered to be promising. However, relatively deep waters around Japan even at close shorelines require us to develop a floating foundation for supporting a wind turbine on top of it. Thus, the Ministry of the Environment (MoE) has kicked off this demonstration project of a floating offshore wind turbine for six years since 2010 FY. As the first phase of the project, a half-scale model supporting a 100 kW wind turbine on top of spar-type foundation was installed offshore of Kabashima Island, Goto city, Nagasaki prefecture, Japan, on June 11th, 2012 as the first grid-connected floating offshore wind turbine in Japan. The spar-type foundation has a unique feature, that is, the upper part is made of steel as usual, but the lower part is made of precast prestressed concrete (PC). Such a configuration is referred to as hybrid-spar in this paper.

During the one-year deployment, a very strong typhoon, named Sanba (international designation: 1216), attacked the half-scale model, but it survived with no damage. The dynamic behavior during the typhoon event is reported in Utsunomiya et al. [1] and Ishida et al. [2]. The dynamic behavior at power generation is also presented in Utsunomiya et al. [3].

After a one-year at-sea test of the half-scale model, the full-scale model supporting a 2MW wind turbine was installed at the same location as the half-scale model on October 18, 2013. The opening ceremony of the power station using the first multi-megawatt floating wind turbine in Japan was held on October 28, 2013. In this paper, the design methodology of the hybrid spar for the full-scale model is presented. Basically, “Guidelines for Floating Offshore Wind Turbine Structures” issued by ClassNK [4] is followed, and the design has been certified by ClassNK. Also, the installation procedure is presented briefly in this paper.

ENVIRONMENTAL CONDITIONS

Wind Conditions

The extreme wind speed at the hub height with a return period of 50 years must be evaluated as part of the design basis. Here, the nonlinear wind climate simulation model MASCOT (Microclimate Analysis System for COmplex Terrain) was used for assessing the extreme wind speed at the site. Figure 1 shows location of the demonstration site offshore of Kabashima Island and the terrain model used in the numerical simulation of wind

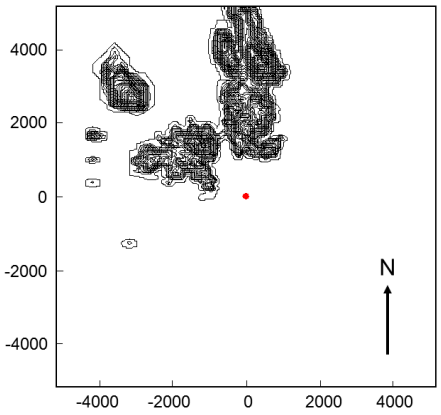

FIGURE 1. LOCATION OF THE DEMONSTRATION SITE AND NUMERICAL TERRAIN MODEL (IN METERS)

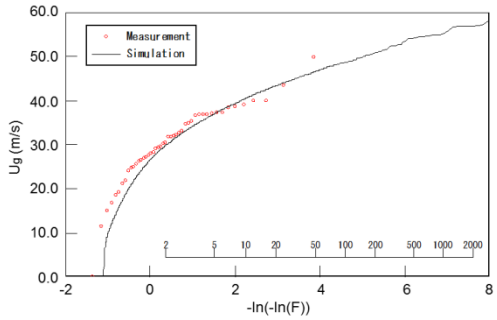

FIGURE 2. ANNUAL MAXIMUM WIND SPEED AS A FUNCTION OF NON-EXCEEDANCE PROBABILITY OBTAINED BY MONTE CARLO SIMULATION OF TYPHOONS

climate. At the origin of Figure 1, the floating wind turbine is to be installed.

Figure 2 shows the results of the annual maximum wind speed as a function of non-exceedance probability obtained by Monte Carlo simulation of typhoons, where 100 typhoons were generated for multiple sets of 100 years (total number of typhoons is 10,000). In Figure 2, the observation data at the site (estimated from the database of the past typhoons) are also plotted. From Figure 2, the gradient wind speed at the gradient height corresponding to a return period of 50 years (F=0.98) can be obtained as 46.7 m/s. Then, the average wind direction for wind speed of 46.7±0.5 m/s was calculated as 154 degrees as shown in Table 1. The wind direction of 154 degrees (wind from SSE direction) was assumed as the wind direction corresponding to the extreme wind speed of a return period of 50 years. For the wind direction of 154 degrees, the effect of complex terrain to the wind speed at the demonstration site was evaluated, and finally the design wind speed of 45.8 m/s at the hub height (H=56 m) was obtained as shown in Table 1. Here, the vertical wind speed profile was assumed to follow the power law given in [5].

The turbulence intensity for the extreme wind speed of a return period of 50 years was determined to be I_1=0.125 (at H=56 m) by following the "Guidelines for Design of Wind

TABLE 1 DESIGN WIND SPEED (10 MINUTES AVERAGE WIND SPEED)

Gradient wind speed	Wind speed (H=56 m)		Wind direction
	Flat terrain	Real terrain	
46.7 m/s	47.0 m/s	45.8 m/s	154 deg. (SSE)

TABLE 2 SCATTER TABLE OF WIND SPEED AT HUB HEIGHT (56 M ABOVE MSL) AND SIGNIFICANT WAVE HEIGHT

Site measurement (1-hour duration)		Significant wave height $H_{1/3}$ [m]										Total	$E[H_{1/3}\|V_{hub}]$ [m]	$E[(H_{1/3})^4\|V_{hub}])^{0.25}$ [m]
		0.25	0.75	1.25	1.75	2.25	2.75	3.25	3.75	4.25	4.75			
1-hour mean wind speed V_{hub} [m/s]	1	66	16	2	0	0	0	0	0	0	0	84	0.37	0.59
	3	645	340	29	10	2	0	0	0	0	0	1026	0.46	0.75
	5	857	583	89	22	9	7	2	0	0	0	1569	0.54	0.98
	7	979	608	138	25	5	5	2	1	0	0	1763	0.54	0.98
	9	766	528	106	31	7	8	6	1	2	0	1455	0.58	1.19
	11	487	269	60	21	5	5	3	3	3	0	856	0.58	1.34
	13	299	190	33	13	10	5	6	2	6	0	564	0.66	1.61
	15	203	105	37	14	5	6	2	2	2	0	376	0.67	1.52
	17	194	68	35	3	3	3	1	3	1	0	311	0.59	1.46
	19	55	44	36	5	1	1	1	2	2	0	147	0.85	1.75
	21	35	15	24	1	1	2	0	3	1	0	82	0.91	1.93
	23	14	6	22	3	0	0	0	2	1	0	48	1.09	2.02
	25	1	2	8	1	0	0	0	0	0	0	12	1.13	1.25
	27	0	0	0	0	0	0	0	1	1	0	2	4.00	4.02
	29	0	0	0	0	0	0	0	0	0	0	0	–	–
	31	0	0	0	0	0	0	0	0	0	0	0	–	–
Total		4601	2774	619	149	48	42	23	20	19	0	8295		

Turbine Support Structures and Foundations" [6]. The turbulence intensity for the Normal Turbulence Model (NTM) was determined to be I_{ref}=0.13, by combining the one-year site-measurement of wind climate onshore of Kabashima Island with the numerical simulation of the turbulence intensity ratios between onshore and offshore locations for each wind direction. The I_{ref} value of 0.13 corresponds to the average of the category B and the category C turbulence intensities defined in IEC 61400-1.

Waves and Current Conditions

Normal Sea State (NSS) The Normal Sea State (NSS) was determined from buoy measurements at the location of the demonstration site for about one year. The wind speed at the offshore demonstration site was estimated by combining the wind speed at the onshore wind mast location (onshore of Kabashima Island) with the numerical simulation of the ratios of wind speed between onshore and offshore locations for each wind direction. Then, since we obtained the simultaneous wind speed and wave height, the scatter table of wind speed and wave height can be obtained as shown in Table 2.

As the Normal Sea State (NSS), the expected value of the wave height conditioned on the concurrent wind speed is necessary. Such a value was obtained by directly using Table 2 (The second column from the right-end of Table 2 shows the expected value of the wave height conditioned on the hub-height wind speed). The sample number in Table 2 is 8295, which corresponds to nearly one year measurement (8760 hours). The significant wave period conditioned on the significant wave height was also determined by using the scatter table of the site measurement.

For evaluation of fatigue (DLC 1.2), the damage equivalent mean wave height considering the effect of the slope m in S-N curve of a steel material (m=3 – 4) was used as shown in the right column of Table 2. Table 2 also shows that the probability

of occurrence of wave height less than 1 m is 0.89, showing that the demonstration site is rather calm in wave height.

Severe Sea State (SSS) The Severe Sea State (SSS) is to be determined as the load effect having a return period of 50 years during power production. However, because of the shortage of the measurement data at the demonstration site, the Extreme Sea State (ESS) unconditioned on the wind speed was used instead. The estimated significant wave height is $H_{1/3}$=7.7 m and the significant wave period is $T_{1/3}$=14 s.

Extreme Sea State (ESS) The significant wave height for a return period of 50 years at the demonstration site is basically 7.7 m as shown above. However, during the typhoon passage of Sanba (1216) near Kabashima Island in 2012, the significant wave height of $H_{1/3}$=9.5 m was recorded at the demonstration site for one hour duration [1]. Since the design wave height of 7.7 m can be considered to correspond to 3 hour duration, it can be converted to 8.4 m for one hour duration by multiplying 1.09 to the value of 7.7 m (IEC 61400-3). Thus, the measured value of 9.5 m in the event of Sanba (1216) exceeded the estimated design wave height of 8.4 m for a return period of 50 years by 13 %. The past 54-years' climate data were used for estimation of the extreme wave height of 7.7 m for a return period of 50 years. The 54 annual maximum wave heights were fitted to a Weibull distribution curve. However, in recent years, the extreme events seem increasing due to the climate change. Such a global trend may be a reason for the underestimation of the extreme wave height.

With observing such a large value in the first year of the deployment to the demonstration site, we have decided to increase the design wave height to some appropriate value by relying on an engineering judgment. Then, the design wave for port/coastal structures was used instead, and the Extreme Sea State (ESS) was increased to $H_{1/3}$=12.1 m and $T_{1/3}$=16.1 s. However, the Severe Sea State (SSS) was kept the same values as the original values of $H_{1/3}$=7.7 m and $T_{1/3}$=14 s.

Tidal Current The current excluding the wind-generated current was estimated as Uss(0)=0.56 m/s at the sea surface from the document survey and the site measurement at the demonstration site. The current velocity distribution in the depth direction was assumed to follow the power law with the power law coefficient of 1/7 as specified in ClassNK guideline [4].

Wind-generated Current The wind-generated current velocity at the sea surface was estimated as 1 % of the 1-hour mean wind speed at 10 m height as specified in ClassNK guideline [4]. The depth dependency of the current velocity was also assumed to follow the ClassNK guideline, i.e., a linear distribution up to 20 m water depth.

DESIGN LOAD CASES

The Design Load Cases (DLCs) were also set-up by following the ClassNK guideline [4]. However, considering the past certification made for the wind turbine used here (Hitachi HTW 2.0-80) and the preliminary analysis results, several design load cases were omitted for extracting design loads of the spar and the tower structures. The design load cases used here are shown in Table 3.

As seen in Table 3, the wind speeds of V_{hub}=12 m/s and 25 m/s were used for design load cases during power production where the ultimate limit state is to be assessed (Type of analysis is designated by "U"). On the other hand, every wind speed at the interval of 2 m/s was used for design load cases to be used for assessment of the fatigue limit sate (Type of analysis is designated by "F"). Here, it is noted that DLC 1.1 and DLC 1.2 were calculated independently because of the difference of current, wave height and wave period at the same wind speed. In particular, DLC 1.1 requires the extrapolation of the loads to a return period of 50 years, which was a cumbersome task in actual computation, because a large number of simulations were needed although the impact to the design load for the spar structure was minimal. No survival load case (as is given in ABS guide [8]) is required in ClassNK guideline [4].

Since the wind turbine used here (Hitachi HTW 2.0-80) is a downwind turbine, it is assured that it is in a free yaw state in the parked situation even at the loss of electrical network. Thus, DLCs 6.2 and 6.3 can be omitted from the design load cases. On the other hand, DLC 7.1 assumed the yaw-fixed case as one of the most severe fault condition to be assessed.

The numerical simulations (the method of simulations is presented in [7]) were basically made for the duration of 60 minutes. Thus, the conversion of V_{hub}=0.95V_{ref} for the hub-height extreme wind speed was made (the conversion of a 10-minutes mean wind speed to a 1-hour mean wind speed). Similarly, the significant wave height for the Extreme Sea State (ESS) was multiplied by 1.09 for conversion of a 3-hour duration value to a 1-hour duration value.

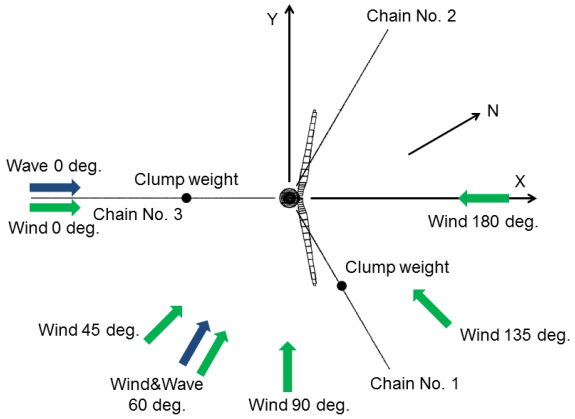

FIGURE 3. PLANVIEW OF DYNAMIC ANALYSIS MODEL AND WIND AND WAVE DIRECTIONS

TABLE 3 DESIGN LOAD CASES

Design situation	DLC	Wind				Wave				Current			Water level		Simulation		Type of analysis	Partial Safety Factor
		model	Vhub	σi	Wind direc	model	$H_{1/3}$	$T_{1/3}$	Wave direc	model	Uwind	Uss	model	depth	Duration	Seeds		
	[−]	[−]	[m/s]	[m/s]	[deg]	[−]	[m]	[s]	[deg]	[−]	[m/s]	[m/s]	[−]	[m]	[min]	[−]		
Power Production	1.1	NTM	12.0	1.9	0	NSS	0.6	5.6	0	NCM	0.09	0.00	MSL	97.2	10	32	U	1.25
		NTM	25.0	3.2	0	NSS	1.1	6.3	0	NCM	0.20	0.00	MSL	97.2	10	32	U	1.25
	1.2	NTM	6.0	1.3	0	NSS	1.0	6.2	0	No	0.00	0.00	NWLR	97.2	60	1	F	1.00
		NTM	8.0	1.5	0	NSS	1.1	6.3	0	No	0.00	0.00	NWLR	97.2	60	1	F	1.00
		NTM	10.0	1.7	0	NSS	1.3	6.5	0	No	0.00	0.00	NWLR	97.2	60	1	F	1.00
		NTM	12.0	1.9	0	NSS	1.5	6.6	0	No	0.00	0.00	NWLR	97.2	60	1	F	1.00
		NTM	14.0	2.1	0	NSS	1.6	6.6	0	No	0.00	0.00	NWLR	97.2	60	1	F	1.00
		NTM	16.0	2.3	0	NSS	1.5	6.6	0	No	0.00	0.00	NWLR	97.2	60	1	F	1.00
		NTM	18.0	2.5	0	NSS	1.6	6.6	0	No	0.00	0.00	NWLR	97.2	60	1	F	1.00
		NTM	20.0	2.7	0	NSS	1.8	6.7	0	No	0.00	0.00	NWLR	97.2	60	1	F	1.00
		NTM	22.0	2.9	0	NSS	2.0	7.3	0	No	0.00	0.00	NWLR	97.2	60	1	F	1.00
		NTM	24.0	3.1	0	NSS	1.6	6.6	0	No	0.00	0.00	NWLR	97.2	60	1	F	1.00
	1.3	ETM	12.0	2.9	0	NSS	0.6	5.6	0	NCM	0.09	0.00	MSL	97.2	60	1	U	1.35
		ETM	25.0	3.7	0	NSS	1.1	6.3	0	NCM	0.20	0.00	MSL	97.2	60	1	U	1.35
	1.4	ECD(−)	10.0	−	change	NSS	0.6	5.6	0	NCM	0.08	0.00	MSL	97.2	1	1	U	1.35
		ECD(+)	10.0	−	change	NSS	0.6	5.6	0	NCM	0.08	0.00	MSL	97.2	1	1	U	1.35
		ECD(−)	12.0	−	change	NSS	0.6	5.6	0	NCM	0.09	0.00	MSL	97.2	1	1	U	1.35
		ECD(+)	12.0	−	change	NSS	0.6	5.6	0	NCM	0.09	0.00	MSL	97.2	1	1	U	1.35
		ECD(−)	14.0	−	change	NSS	0.7	5.7	0	NCM	0.11	0.00	MSL	97.2	1	1	U	1.35
		ECD(+)	14.0	−	change	NSS	0.7	5.7	0	NCM	0.11	0.00	MSL	97.2	1	1	U	1.35
	1.5	EWS(H−)	12.0	−	0	NSS	0.6	5.6	0	NCM	0.09	0.00	MSL	97.2	1	1	U	1.35
		EWS(H+)	12.0	−	0	NSS	0.6	5.6	0	NCM	0.09	0.00	MSL	97.2	1	1	U	1.35
		EWS(V+)	12.0	−	0	NSS	0.6	5.6	0	NCM	0.09	0.00	MSL	97.2	1	1	U	1.35
		EWS(H−)	25.0	−	0	NSS	1.1	6.3	0	NCM	0.20	0.00	MSL	97.2	1	1	U	1.35
		EWS(H+)	25.0	−	0	NSS	1.1	6.3	0	NCM	0.20	0.00	MSL	97.2	1	1	U	1.35
		EWS(V+)	25.0	−	0	NSS	1.1	6.3	0	NCM	0.20	0.00	MSL	97.2	1	1	U	1.35
	1.6	NTM	12.0	1.9	0	SSS	7.7	14.0	0	NCM	0.09	0.00	NWLR	97.2	60	6	U	1.35
		NTM	25.0	3.2	0	SSS	7.7	14.0	0	NCM	0.20	0.00	NWLR	97.2	60	6	U	1.35
Parked	6.1	EWM	43.5	5.9	0	ESS	13.2	16.1	0	ECM	0.36	0.56	EWLR	95.6	60	6	U	1.35
		EWM	43.5	5.9	45	ESS	13.2	16.1	0	ECM	0.36	0.56	EWLR	95.6	60	6	U	1.35
		EWM	43.5	5.9	90	ESS	13.2	16.1	0	ECM	0.36	0.56	EWLR	95.6	60	6	U	1.35
		EWM	43.5	5.9	135	ESS	13.2	16.1	0	ECM	0.36	0.56	EWLR	95.6	60	6	U	1.35
		EWM	43.5	5.9	180	ESS	13.2	16.1	0	ECM	0.36	0.56	EWLR	95.6	60	6	U	1.35
		EWM	43.5	5.9	60	ESS	13.2	16.1	60	ECM	0.36	0.56	EWLR	95.6	60	6	U	1.35
		EWM	43.5	5.9	0	ESS	13.2	16.1	0	ECM	0.36	0.56	EWLR	99.7	60	6	U	1.35
	6.4	NTM	3.0	1.0	0	NSS	0.8	5.9	0	No	0.00	0.00	NWLR	97.2	60	1	F	1.00
		NTM	28.0	3.5	0	NSS	4.8	10.1	0	No	0.00	0.00	NWLR	97.2	60	1	F	1.00
		NTM	32.0	3.8	0	NSS	4.8	10.1	0	No	0.00	0.00	NWLR	97.2	60	1	F	1.00
Parked and fault conditions	7.1	EWM	34.8	4.8	0	ESS	5.2	10.1	0	ECM	0.29	0.47	NWLR	97.2	60	6	U	1.10
		EWM	34.8	4.8	90	ESS	5.2	10.1	0	ECM	0.29	0.47	NWLR	97.2	60	6	U	1.10
		EWM	34.8	4.8	180	ESS	5.2	10.1	0	ECM	0.29	0.47	NWLR	97.2	60	6	U	1.10

The wind and wave directions were set as shown in Figure 3 and Table 3. Basically, the misalignment angles between wind and wave directions were assessed at 0, 45, 90, 135 and 180 degrees for DLC 6.1. The wind-generated current was assumed to be parallel to the wind direction (as specified in ClassNK guideline [4]). On the other hand, the tidal current was assumed to be parallel to the wave direction (the tidal current flows in the same direction as the wave propagation direction, as specified in ClassNK guideline [4]).

In Figure 3, the wind direction at other than 0 degree shows the wind flow at the misaligned angle with the rotor axis. However, in the dynamic simulation, the rotor easily rotates because of the free-yaw system, and the rotor axis becomes almost in the parallel direction to the wind direction at an early stage of the dynamic simulation.

LOAD ANALYSIS

Method of Load Analysis

Figure 4 shows the main dimensions of the full-scale model. The spar outer diameter at the main part is 7.8 m, and that at the water line is 4.8 m. The design draft is 76 m with the hub height of 56 m. It is moored by three anchor chains, in which two of them are equipped with clump weights. The reason why one of the chains is not equipped with clump weights is because severe wave direction is restricted only from east – south – west directions, and thus the north mooring line can be designed lighter than the other two lines.

Figure 5 shows the dynamic analysis model used in the simulation. The simulation tool is basically the same as reported in [7]. That is, the aero-hydro-servo-mooring dynamics-elasticity coupling is all considered in the simulation

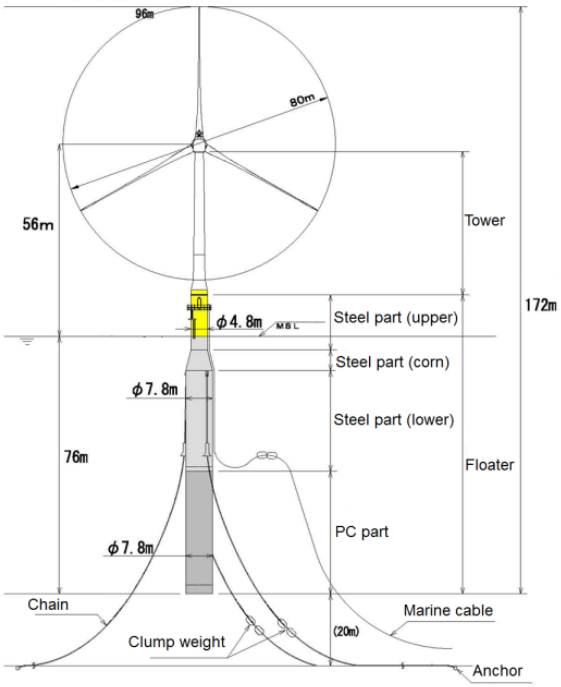

FIGURE 4. MAIN DIMENSIONS OF THE FULL-SCALE MODEL

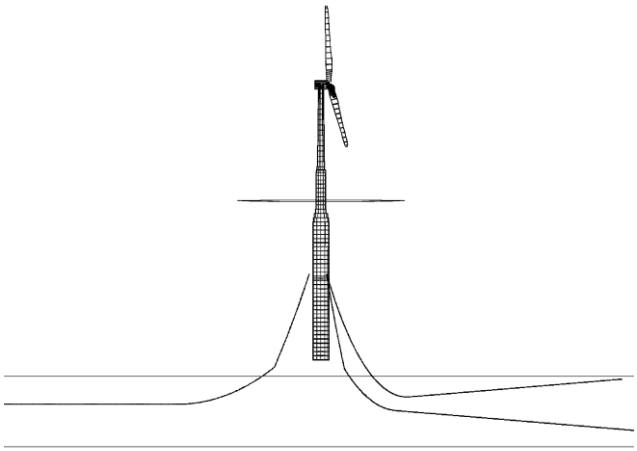

FIGURE 5. DYNAMIC ANALYSIS MODEL

TABLE 4 EXAMPLE OF SUMMARY TABLE OF SECTION LOADS (AT TOWER BASE SECTION)

No.			L.F.	Fx	Fy	Fz	Fxy	Mx	My	Mz	Mxy
[−]			[−]	[kN]	[kN]	[kN]	[kN]	[kNm]	[kNm]	[kNm]	[kNm]
6	Fx	Max	1.35	2382	−68	−1576	2383	2728	83485	−402	83530
		Min	1.35	−2112	88	−2073	2114	−2906	−76922	−115	76977
	Fy	Max	1.35	1061	1990	−1560	2255	−69691	36721	−422	78774
		Min	1.35	−534	−916	−2083	1060	31950	−19169	69	37259
	Fz	Max	1.35	1869	−44	−1474	1870	1554	64761	−135	64779
		Min	1.35	−278	−12	−2326	278	1039	−8307	−77	8372
	Fxy	Max	1.35	2382	−68	−1576	2383	2728	83485	−402	83530
		Min	1.35	0	0	−2064	0	−224	1173	98	1194
	Mx	Max	1.35	−534	−916	−2083	1060	31950	−19169	69	37259
		Min	1.35	1061	1990	−1560	2255	−69691	36721	−422	78774
	My	Max	1.35	2382	−68	−1576	2383	2728	83485	−402	83530
		Min	1.35	−2112	88	−2073	2114	−2906	−76922	−115	76977
	Mz	Max	1.35	464	349	−2007	581	−10987	21129	2625	23814
		Min	1.35	354	−20	−1910	355	1900	14055	−3368	14182
	Mxy	Max	1.35	2374	−87	−1589	2376	3616	83458	−386	83536
		Min	1.35	31	30	−2008	43	0	−11	417	11

program. As a solver of the multibody dynamics model, the commercially available program MSC.Adams was used. For numerical simulation of DLC 6.1, the mooring lines were also modeled as a dynamic model composed of lumped mass-springs. The added mass and damping forces acting on the mooring lines were also taken into account. On the other hand, the numerical simulations other than DLC 6.1 were analyzed using a quasi-static model of the mooring lines based on the static catenary theory. In fact, this is more computationally efficient than that using dynamic mass-spring model.

Load Analysis Results

For all design load cases shown in Table 3, time domain simulations were made. By the dynamic simulation, the section loads acting at each section along the axis of the spar and tower can be obtained as time series data. From the time series data, statistical values such as maximum value, minimum value, mean and standard deviation of each section load can be extracted. Then, at one particular section of the spar and the tower, all of the maximum and minimum values are compared among those from all DLCs, and the largest maximum and the smallest minimum values are extracted at each section. Table 4 shows an example of such a summary table at tower base section. Here, F_x and F_y represent the shearing forces acting along X and Y axes of the section, F_z the axial force along the spar axis (Z-axis), F_{xy} the shearing force resultant, M_x and M_y the bending moments acting around X and Y axes, M_z the torsional moment around the spar axis, and M_{xy} the bending moment resultant. In the table, the simultaneous values of the section loads are also indicated. Note that in Table 4, all values other than Max of M_z and Min of M_z occurred for DLC 6.1. Max of M_z and Min of M_z occurred for DLC 1.4. Basically, DLC 6.1 is the most important design load case that controls the structural design of this particular spar model.

DESIGN VERIFICATION

Design Verification for Ultimate Limit State

The spar and the tower structures are basically made as a simple cylindrical shell structure with ring stiffeners. Then, the ultimate strength may be estimated rather simply based on the section loads. Here, the ultimate strength check was made line by line using the summary table of the section loads as shown in Table 4. For the tower sections, “Guidelines for Design of Wind Turbine Support Structures and Foundations” [6] was used as the basis of the design verification. For the spar sections (steel part), API RP2A-WSD [9] was followed. Since the section loads to be used for ultimate strength check were multiplied by the load factor (basically 1.35), the allowable stress was increased with the ratio of 1/3 as specified in 3.3.5 Safety Factors in [9].

Design Verification for Fatigue Limit State

For design verification for fatigue limit state, the stresses at detailed portions (e.g., at welding portions) are necessary. Thus, the simplified method used for design verification for ultimate

FIGURE 6. FABRICATION OF THE CONCRETE SEGMENTS

FIGURE 7. TRANSPORTATION OF THE STEEL PART

limit state cannot be used. Here, by using a detailed FEM model of the specified portion, the linear relationships between the section loads at the sections and the stress to be evaluated for the fatigue were first evaluated. Then, by using the time series of the section loads and the linear relationships between the section loads and the stress, the time series of the stress at a particular location was generated. The stress range was then counted by using the rain-flow method, and finally the cumulative damage ratio due to fatigue was obtained. In this particular analysis, DNV RP-C203 [10] was followed.

Design Verification for Mooring System

The tensions acting on the mooring lines and the loads acting at the anchors were also evaluated by the dynamic simulation simultaneously in the load analysis for all DLCs given in Table 3. At the same time, dynamic simulation for one-line break of mooring line was also made. The governing load case for the mooring design was DLC 6.1.

For the anchor chains, the safety factor of 1.67 was used for verification of the maximum tension for the intact state [4]. For the one-line break case, the remaining chains were checked against the safety factor of 1.05 in the transient state and 1.25 in the stationary state in the new equilibrium position moored only by two mooring lines. For the check of one-line break case, the environmental conditions for a return period of one year were

FIGURE 8. CONSTRUCTION OF THE PC PART OF THE SPAR STRUCTURE

FIGURE 9. THE HYBRID SPAR STRUCUTER IN COMPLETION

used [4].

For the anchors, the safety factor of 1.50 was used for the intact state, and 1.0 for the one-line break case. The test load to the anchors was determined as the maximum tension load at the anchor point in the intact state.

CONSTRUCTION

The precast prestressed concrete (PC) segments were fabricated in a factory of Hume pipe at Kitakyushu city, Fukuoka prefecture. The precast segments were fabricated as a 1/4 part of the circular section (outer diameter: 7.8 m) with the height of 2 m because of the restrictions for land transportation (Figure 6). After the accelerated curing with vapor, the demolding, and the air curing, the completed PC segments were transported to the construction quay at Matsuura city, Nagasaki prefecture by using conventional truck transportation.

At the same time, the steel part of the spar structure was fabricated at a shipyard for offshore structures in Sakai city, Osaka prefecture. The completed steel part was then transported to the same construction quay at Matsuura city by

FIGURE 10. DRY-TOWING OF THE SPAR STRUCTURE

FIGURE 11. UPENDING OF THE SPAR STRUCTURE

FIGURE 12. ASSEMBLY OF THE ROTOR

FIGURE 13. DEPLOYMENT OF THE ANCHOR AND CHAINS

FIGURE 14. TOWING TO THE DEMONSTRATION SITE

FIGURE 15. HOOK-UP OF THE CHAINS

FIGURE 16. GENERAL VIEW OF THE FULL-SCALE MODEL IN COMPLETION

using a conventional barge (Figure 7).

At the construction quay in Matsuura city, four segments were firstly joined together to form a ring-shaped part with the outer diameter of 7.8 m and the height of 2 m in the horizontal position. The completed ring-shaped parts were then assembled together to form a circular cylinder by using post-tensioning steel bars for the bottom half of the spar structure (Figure 8).

After the completion of the PC part of the spar structure, the upper steel part was joined to the lower PC part by using a floating crane. Figure 9 shows the general view of the hybrid spar structure in completion in the horizontal position.

INSTALLATION

The completed hybrid-spar structure was dry-towed to the north area of the Kabashima Island, where the wave conditions are gentler than those at the demonstration site (south of the Kabashima Island) (Figure 10).

Then, the hybrid-spar structure was upended with the help of a floating crane as shown in Figure 11. After completion of the upending, the sea water was filled to stabilize the spar at the designed draft. Then, the solid ballasting material was filled, where part of the sea water was replaced by the solid ballast. Even during the expected short periods of the construction at the north area of the Kabashima Island, there was a risk to be attacked by severe typhoons during the construction there. Thus, the temporary mooring system was designed for the environmental conditions with a return period of 10 years.

The tower sections (divided in two pieces), the nacelle, and the rotor were then assembled by using a floating crane (Figure 12).

At the demonstration site, the anchor and the chains were deployed beforehand, and the test load was applied for each of three mooring lines (Figure 13).

Having a weather window of more than three days, the temporary moorings at the north construction area were unhooked. Then, the floating wind turbine structure was towed to the demonstration site by using two tug-boats (Figure 14). As soon as it arrived at the demonstration site, the pre-laid anchor chains were hooked-up to the spar structure (Figure 15).

Final hook-up of the mooring chains was completed on October 18, 2013. After connection of the marine cable for the grid-connection (which was also used for the half scale model), it began to operate from October 28, 2013, as the first multi-megawatt floating offshore wind turbine in Japan (Figure 16).

CONCLUSIONS

In this paper, outline of the design method for spar-type floating offshore wind turbine structure was presented. As shown in the paper, the spar structure presented here can be modelled as a simple one-dimensional structure; thus, the section loads along the longitudinal axis of the spar and the tower structure can be directly assessed and verified by using a summary table (as seen in Table 4). On the other hand, the fatigue limit state should be evaluated using a local stress at the specified point, which requires us to generate stress time-series data from the section loads time-series data.

Construction and installation procedures are also briefly presented. Basically, the design, construction, and installation have been made with a great success. However, still further cost reduction is necessary for vast utilization of the same system as part of commercial power plant in near future.

ACKNOWLEDGMENTS

This work is a part of the floating offshore wind turbine demonstration project by Ministry of the Environment of Japan.

REFERENCES

[1] Utsunomiya, T., Sato, I., Yoshida, S., Ookubo, H., and Ishida, S., 2013, “Dynamic Response Analysis of a Floating Offshore Wind Turbine During Severe Typhoon Event,” Proceedings of 32nd International Conference on Ocean, Offshore and Arctic Engineering, Nantes, France, OMAE2013-10618.

[2] Ishida, S., Kokubun, K., Nimura, T., Utsunomiya, T., Sato, I., and Yoshida, S., 2013, “At-sea Experiment of a Hybrid Spar Type Offshore Wind Turbine,” Proceedings of 32nd International Conference on Ocean, Offshore and Arctic Engineering, Nantes, France, OMAE2013-10655.

[3] Utsunomiya, T., Yoshida, S., Kiyoki, S., Sato, I., and Ishida, S., 2014, “Dynamic Response of a Spar-type Floating Wind Turbine at Power Generation,” Proceedings of 33rd International Conference on Ocean, Offshore and Arctic Engineering, San Francisco, California, USA, OMAE2014-24693.

[4] ClassNK, 2012, “Guidelines for Floating Offshore Wind Turbine Structures,” first edition, June 2012.
[5] Meng, Y., Matsui, M., and Hibi, K., 1996, “Characteristics of the Vertical Wind Profile in Neutrally Atmospheric Boundary Layers, Part 2: Strong Winds during Typhoon Climates,” J. of Wind Engineering, Japan Association for Wind Engineering, No. 66, pp. 3-14, 1996.
[6] Ishihara, T. (Ed.), 2010, “Guidelines for Design of Wind Turbine Support Structures and Foundations,” JSCE, December 2010.
[7] Utsunomiya, T., Yoshida, S., Ookubo, H., Sato, I., and Ishida, S., 2014, “Dynamic Analysis of a Floating Offshore Wind Turbine Under Extreme Environmental Conditions,” Journal of Offshore Mechanics and Arctic Engineering, Vol. 136, pp. 020904-1 - 11.
[8] ABS, 2014, “Guide for Building and Classing Floating Offshore Wind Turbine Installations,” July 2014.
[9] API, 2000, “Recommended Practice for Planning, Designing and Constructing Fixed Offshore Platforms – Working Stress Design,” RP 2A-WSD with Errata and Supplement 3, Oct 2007.
[10] DNV, 2012, “Fatigue Design of Offshore Steel Structures,” DNV-RP-C203, Oct 2012.